ISSN 1063-7761, Journal of Experimental and Theoretical Physics, 2016, Vol. 122, No. 5, pp. 874–882. © Pleiades Publishing, Inc., 2016.
Original Russian Text © A.B. Batdalov, A.M. Aliev, L.N. Khanov, V.D. Buchel'nikov, V.V. Sokolovskii, V.V. Koledov, V.G. Shavrov, A.V. Mashirov, E.T. Dil'mieva, 2016, published in Zhurnal Eksperimental'noi i Teoreticheskoi Fiziki, 2016, Vol. 149, No. 5, pp. 1011–1021.

ORDER, DISORDER, AND PHASE TRANSITION IN CONDENSED SYSTEM

Magnetic, Thermal, and Electrical Properties of an $Ni_{45.37}Mn_{40.91}In_{13.72}$ Heusler Alloy

A. B. Batdalov[a], A. M. Aliev[a]*, L. N. Khanov[a], V. D. Buchel'nikov[b], V. V. Sokolovskii[b, c], V. V. Koledov[d], V. G. Shavrov[d], A. V. Mashirov[d], and E. T. Dil'mieva[d]

[a] *Amirkhanov Institute of Physics, Dagestan Research Center, Russian Academy of Sciences, ul. 26 Bakinskikh komissarov 94, Makhachkala, Dagestan, 367003 Russia*

[b] *Chelyabinsk State University, ul. Brat'ev Kashirinykh 129, Chelyabinsk, 454001 Russia*

[c] *National University of Science and Technology MISiS, Leninskii pr. 4, Moscow, 119049 Russia*

[d] *Institute of Radio Engineering and Electronics, Russian Academy of Sciences, ul. Mokhovaya 18, Moscow, 125009 Russia*

**e-mail: lowtemp@mail.ru*

Received March 29, 2015

Abstract—The magnetization, the electrical resistivity, the specific heat, the thermal conductivity, and the thermal diffusion of a polycrystalline Heusler alloy $Ni_{45.37}Mn_{40.91}In_{13.72}$ sample are studied. Anomalies, which are related to the coexistence of martensite and austenite phases and the change in their ratio induced by a magnetic field and temperature, are revealed and interpreted. The behavior of the properties of the alloy near Curie temperature T_C also demonstrates signs of a structural transition, which suggests that the detected transition is a first-order magnetostructural phase transition. The nontrivial behavior of specific heat detected near the martensite transformation temperatures is partly related to a change in the electron density of states near the Fermi level. The peculiar peak of phonon thermal conductivity near the martensitic transformation is interpreted as a consequence of the appearance of additional soft phonon modes, which contribute to the specific heat and the thermal conductivity.

DOI: 10.1134/S1063776116040129

INTRODUCTION

Heusler alloys are characterized by a sequence of magnetic, structural, and modulation phase transitions, which can be controlled by external fields, and a set of functional properties, which are promising for applications related to these transitions [1]. Moreover, Heusler alloys are excellent model objects to study the physical properties of strongly correlated electronic systems.

Although Heusler alloys have attracted close attention of researchers, many problems still need to be refined. For example, nonstoichiometric Ni–Mn–X (X = In, Sb, Sn) alloys undergo unusual magnetic–structural phase transitions from a high-temperature ferromagnetic phase into a low-temperature with a weak or zero magnetization. This phenomenon can be explained in terms of several concepts. The first concept implies that this phenomenon is caused by the inversion of the sign of exchange interaction, which occurs along with the structural austenite–martensite transition and is accompanied by the transformation of a sample into an antiferromagnetic state with zero magnetization [2]. The results obtained for the Ni–Mn–In system [3] demonstrate that the phase transition from a high-temperature ferromagnetic phase into a low-temperature paramagnetic phase takes place in these alloys. However, according to [4, 5], the behavior of low-temperature magnetization is associated with the transformation of a sample into a ferrimagnetic state.

Therefore, any information that can elucidate these and other features of the phase transitions in Ni–Mn–In alloys is important, since it can serve as a solid argument for a certain model of explaining the detected anomalies. Practical interest in these materials is mainly related to the unusually high elastic strains that appear during martensitic transformations and a high magnetocaloric effect (MCE) in the range of magnetic–structural phase transitions [1].

Since both magnetic strain and MCE are caused by a strong relation between the magnetic, electron, and lattice subsystems, to study the influence of this relation on the electrical, magnetic, and thermophysical properties of Ni–Mn–In Heusler alloys is an important and challenging problem.

The purpose of this work is to experimentally investigate the magnetization (M), the electrical resistivity (ρ), the specific heat (C_p), the thermal diffusion (η), and the thermal conductivity (k) of a polycrystalline $Ni_{45.37}Mn_{40.91}In_{13.72}$ sample.

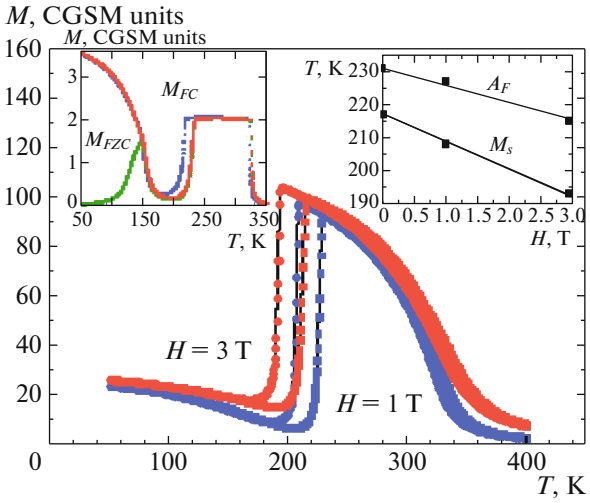

Fig. 1. (Color online) Magnetization of an $Ni_{45.37}Mn_{40.91}In_{13.72}$ Heusler alloy upon heating and cooling in various magnetic fields. (left-hand inset) Magnetization in a field of 0.005 T and (right-hand inset) shift of the martensite transformation temperatures in a magnetic field.

EXPERIMENTAL

The sample to be studied was fabricated by arc melting in an argon atmosphere and was then subjected to homogenizing annealing at $T = 900°C$ for 48 h in vacuum. The initial nominal charge composition corresponded to the chemical formula $Ni_{46}Mn_{41}In_{14}$, and the actual composition determined by energy dispersive spectroscopy corresponded to the formula $Ni_{45.37}Mn_{40.91}In_{13.72}$. The necessity of determining the exact elemental composition of the sample was related to the fact that the physical properties of Heusler alloys are extremely sensitive to a change in the elemental composition [6].

The magnetization of the sample was measured on a Quantum Design PPMS-9T device, the electrical resistivity was measured by the four-probe method, the thermal conductivity was determined by the steady thermal flow method, and the specific heat and the thermal diffusion were determined with ac calorimetry [7]. Moreover, data on specific heat C_p and thermal diffusion η were used to determine thermal conductivity k, since they are interrelated as

$$k = \frac{d}{M} C_p \eta, \qquad (1)$$

where d is the sample density and M is the molar mass of the sample. The values of thermal conductivity k determined by both methods agreed well with each other. As temperature sensors, we used copper–constantan and chromel–constantan thermocouples. The sample was heated to a temperature above T_C before every measurement.

RESULTS AND DISCUSSION

Figure 1 shows the temperature dependence of the magnetization measured at various magnetic fields upon heating and cooling. As the temperature decreases, an sharp increase in the magnetization is detected in the austenite phase, which is related to the transformation of the sample into a ferromagnetic state (Fig. 1, left-hand inset). The maximum rate of change of the magnetization with temperature is detected at $T_C = 319$ K upon cooling and at $T_C = 322$ K upon heating, which corresponds to the Curie temperature. A well-pronounced temperature hysteresis, which can indicate structural changes that accompany this transformation, is observed in this temperature range. Based on the measured magnetic and structural properties of an $Ni_{50}Mn_{35}In_{15}$ alloy, the authors of [4, 5] assumed that a structural transition from paramagnetic austenite into ferromagnetic martensite, which can be identified as a magnetostructural first-order phase transition, also takes place at T_C. However, this and other conclusions drawn in [4, 5] (maximum in the field magnetization curve was related to a spin-flip transition, and low-temperature weak magnetization, to the transformation of a sample into a ferrimagnetic state) make it necessary to introduce substantial corrections to the generally accepted concepts of the magnetic and structural transitions in Ni–Mn–In alloys. To refine this problem, we performed precise measurements of specific heat $C_p(T)$ and magnetization $M(T)$ near T_C upon heating and cooling at various rates of change of temperature (0.4–1.0) K/min (Figs. 2a, 2b). The results of these measurements revealed a hysteresis in the behavior of $C_p(T)$ and $M(T)$; therefore, the conclusions drawn in [4, 5] seem to be supported. Note that the hysteresis width depends on the rate of change of temperature, decreasing with decreasing temperature. Our differential scanning calorimetry data obtained on a sample with a close composition ($Ni_{49.3}Mn_{40.4}In_{10.3}$) also demonstrate signs of a first-order phase transition near T_C (Fig. 2c). However, this phase transition is not a classical first-order phase transition, since no sharp complete transformation of the sample into another crystal structure takes place here.

According to [4], X-ray diffraction data demonstrate that reflections of both martensite and austenite phases are present in the temperature range from T_C to the temperature of the maximum in the magnetization curve; that is, the structure of the system is heterogeneous in this temperature range. obviously, additional investigations are necessary to reveal the nature of the phase transition at the Curie point.

As T decreases further, M remains constant over a wide temperature range (Fig. 1, left-hand inset). Two anomalies, which are related to the onset of the martensitic transformation ($M_s = 217$ K) and the end of the reverse transformation into the austenite phase ($A_f =$

231 K), are clearly visible in the low-temperature range. The values of M_f (end of the martensitic transformation) and A_s (onset of the reverse martensite–austenite transformation) obtained from an analysis of the $M(T)$ curves in weak fields at low temperatures are 207 and 215 K, respectively.

As is seen in Fig. 1, the magnetization of the martensite phase does not vanish with decreasing T; that is, the alloy is still weakly magnetic. The further decrease in the temperature in weak fields is characterized by the appearance of a magnetically ordered phase with $T_C^M \approx 170$ K and by the splitting of the $M(T)$ curves: $M_{FC}(T)$ exhibits a monotonic increase, whereas $M_{ZFC}(T)$ passes through a maximum. This behavior is characteristic of the alloys that have a magnetic disorder and an antiferromagnetic interaction.

There are examples where the magnetization of the martensite phase in an Ni–Mn–In alloy becomes almost zero in weak fields and remains very low down to extremely low temperatures [8, 9], and there are cases where it is weakly magnetic [10, 11]. Moreover, a more complex $M(T)$ dependence is also detected: the magnetization becomes zero after the end of the martensitic transformation and begins to grow when temperature decreases further, as in our case. This behavior resembles the paramagnet–ferromagnet transition in martensite with its specific Curie temperature T_C^M [12, 13].

Based on the existing data, it is difficult to unambiguously answer the question about the cause of the behavior of magnetization at low temperatures. This was also noted by the authors of recent work [14], who mentioned that the problem of the type of magnetic ordering in the martensite of Ni–Mn–In alloys is still an open question. Nevertheless, taking into account the obtained $M(T)$ dependence and the results of neutron diffraction of an Ni–Mn–In alloy (unpublished Phina–Ari–Gur data; they unambiguously indicate an antiferromagnetic character of the magnetic ordering in the martensite phase), we can assume the coexistence of weak magnetic and antiferromagnetic interactions in the system [12, 15].

The martensitic transformation temperatures in Heusler alloys depend strongly on a magnetic field, which shift them up or down. A magnetic field increases the magnetization of the phase with a higher magnetization (in this case, austenite) and the shift of M_s toward low temperatures, which is clearly visible in Fig. 1 (where $M(T)$ curves are presented for various magnetic fields). For the Ni–Mn–Ga, the picture is opposite: the magnetization of the martensite phase is higher than the magnetization of austenite; therefore, magnetic field H shifts M_s toward high temperatures [13].

The dependence of martensite transformation temperatures M_s, M_f, A_s, and A_f on the magnetic field follows from the phase equilibrium condition (Clausius–Clapeyron equation)

$$\Delta T = \left(\frac{\Delta M}{\Delta S}\right)\Delta H, \qquad (2)$$

where ΔM is the difference between the magnetizations of austenite and martensite and ΔS is the change of the entropy. Thus, the shifts of the martensite trans-

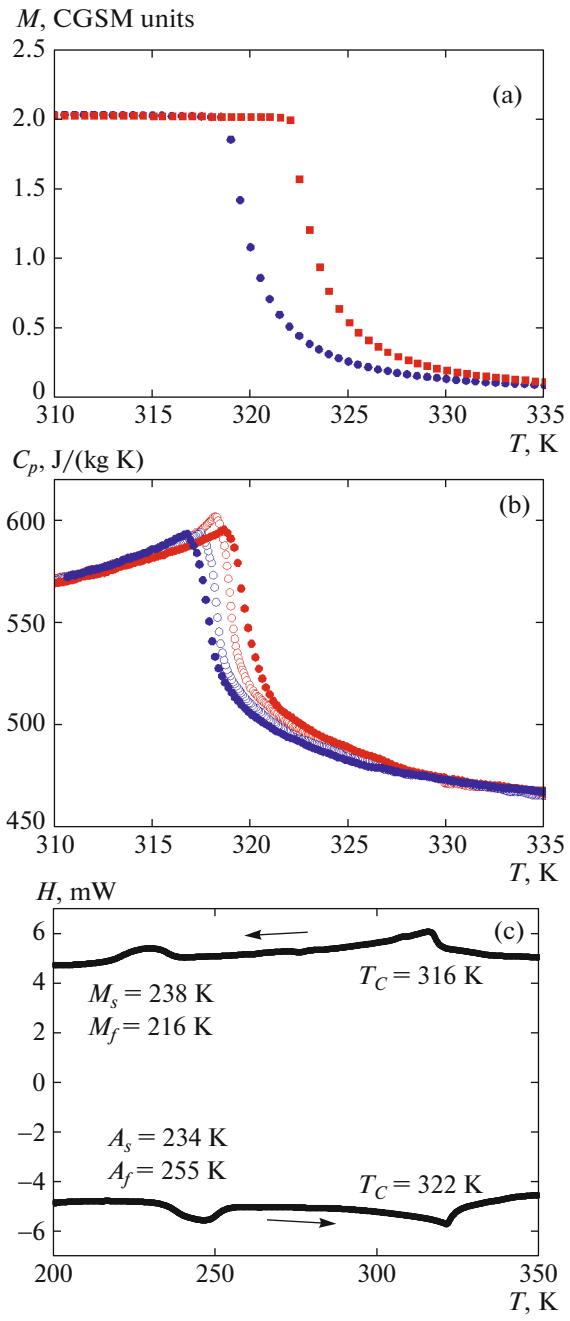

Fig. 2. (Color online) (a) Magnetization, (b) specific heat, and (c) heat flow vs. temperature T_C upon heating and cooling. The hysteresis width in the $C_p(T)$ curve is $\Delta T = 2.1$ K at a rate of change of temperature of 1 K/min and $\Delta T = 0.9$ K at a rate of 0.4 K/min.

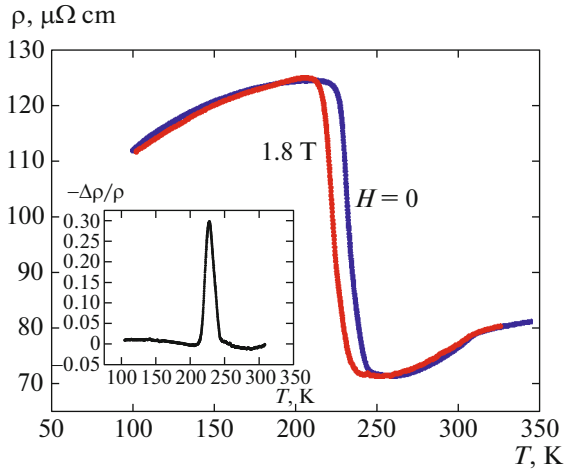

Fig. 3. (Color online) Temperature dependences of the electrical resistivity of $Ni_{45.37}Mn_{40.91}In_{13.72}$ in a magnetic field and a zero magnetic field upon heating. (inset) Temperature dependence of magnetoresistance.

formation temperatures are directly proportional to a change in the magnetic field.

To test this dependence, we plotted martensite transformation temperatures M_s and A_f versus the magnetic field. As is seen in the right-hand inset to Fig. 1, this dependence is linear, $\Delta T/\Delta H = -8$ K/T for M_s and $\Delta T/\Delta H = -6$ K/T for A_f. These values are close to a value of −7 K/T for $Ni_{46}Mn_{41}In_{13}$ [15] and are slightly lower than −12 K/T for $Ni_{50}Mn_{34}In_{16}$ [13]. The estimation of the shift of M_s from Eq. (2) for $\mu_0 H = 1.8$ T using the $M(T)$ data in Fig. 1 and the value of ΔS obtained from an analysis of the specific heat C_p data in this field and without this field yields $\Delta T =$ 20 K, which agrees reasonably with an experimental value of 14 K.

Let us discuss the electrical resistivity results (Fig. 3). As temperature decreases, ρ decreases and exhibits the behavior that is typical of metals; an inflection point takes place at $T_C \approx 320$ K; and a segment of a sharper decrease in the electrical resistivity, which is caused by the disappearance of conduction electron scattering by magnetic order parameter fluctuations, begins [15]. As the temperature decreases further, the electrical resistivity begins to grow sharply near $T \approx 245$ K and almost doubles in the martensite phase, from 70 to 125 μΩ cm. The increase in the electrical resistivity during the austenite–martensite transition is mainly related to the transition of the crystal structure from the highly symmetric cubic phase (austenite) into the distorted tetragonal phase (martensite) with a lower symmetry [9, 16, 17].

In the relaxation time approximation, an expression for $\rho(T)$ has the form

$$\rho(T) = \frac{m^*}{e^2 n\tau}, \qquad (3)$$

where m^* is the effective carrier mass, n is the carrier concentration, and τ is the relaxation time. In principle, all parameters (m^*, n, τ) entering into this expression can be responsible for the increase in the electrical resistivity during the transition into the martensite phase. However, reasonable physical prerequisites for the sharp increase in the effective carrier mass in the martensite phase are thought to be absent, and the sharp growth of the electrical resistivity during the transition into the martensite phase is most likely to be related to both a decrease in the carrier concentration and a change in the mechanism of carrier scattering. This assumption is supported by the data on measuring the electronic specific heat of an $Ni_{50}Mn_{34}In_{16.3}$ alloy [18], according to which the austenite–martensite transformation is accompanied by a more than threefold decrease in the carrier concentration. This result can also be achieved upon the growth of the structural disorder caused by the martensitic transformation or upon additional electron scattering by twin boundaries. There is reason to think all these mechanisms operate in our case and ensure the detected $\rho(T)$ dependence. A relation between the change in the electron density of states at the Fermi level and the $\rho(T)$ dependence of an Ni–Co–Mn–In alloy was also found in [19, 20].

However, a metallic character of the $\rho(T)$ dependence in both the austenitic ferromagnetic phase and the martensite phase points to the fact that the phonon mechanism of carrier scattering is likely not be fully ignored.

Figure 3 (inset) shows the results of measuring the magnetoresistance. First of all note that this is the effect related to the coexistence of two structural phases with different electrical conductivities, the relation between which changes in a magnetic field, rather than the kinetic effect caused by a decrease in the mean free path of carriers in a magnetic field. It is seen that the magnetoresistive effect manifests itself in the range of coexistence of martensite and austenite in the temperature range $T = 220$–240 K.

A magnetic field shifts M_s toward low temperatures, increasing the volume of the austenitic high-conductivity phase and inducing a negative magnetoresistance,

$$\frac{\Delta\rho_0}{\rho_0} = \frac{\rho_H - \rho_0}{\rho_0}.$$

The maximum value ($-\Delta\rho/\rho_0 = 30\%$) was reached in a field $\mu_0 H = 1.8$ T near the martensite transformation temperature ($T = 228$ K). The further decrease of T is accompanied by the disappearance of the magnetoresistive effect, which is thought to be associated with the transformation of the sample into the martensite phase.

The experimental data on specific heat are shown in Fig. 4. The $C_p(T)$ curve has a pronounced characteristic maximum near the paramagnet–ferromagnet

transition. The specific heat peak corresponds to $T = 320$ K, which is taken to be T_C. This temperature approximately coincides with $T_C = 319$ K obtained from an analysis of $M(T)$.

When the temperature decreases further, a sharp specific heat jump, which is caused by the structural austenite–martensite transition, is detected near $T_M = 223$ K. The reverse transition is detected at $T_A = 233$ K and the temperature hysteresis is $\Delta T = 10$ K, which is slightly smaller than it follows from the magnetization data ($\Delta T = 14$ K).

The pronounced asymmetry and a clear steplike character of the specific heat jump near the martensitic transformation have engaged our attention: C_p above the transformation is significantly higher than C_p below the transformation, and no difference in ΔC upon heating and cooling is seen (this difference was detected for an $Ni_{50}M_{27}(In_{0.2}Sn_{0.8})_{13}$ sample and was attributed to the influence of the latent heat of transformation [21]). A small asymmetry was detected for $Ni_{50}Mn_{34}In_{16}$ in [22]. No signs of structural transformations in the $C_p(T)$ curve of a $Ni_{50}Mn_{34}In_{16}$ sample were observed in [23].

The authors of [19] suppose that the asymmetry of the specific heat of an Ni–Co–Mn–In alloy results from an additional contribution of conduction electrons to $C_p(T)$ in the ferromagnetic austenite phase, which agrees with the detected growth of the conductivity in the austenite phase. Indeed, the FM and AFM states in the magnetic alloys that undergo magnetic order–disorder phase transitions, e.g, FeRh alloys, differ mainly in the electron density of states near the Fermi level $N(E_F)$, and the AFM–FM transition in them is accompanied by a sharp increase of $N(E_F)$ and, hence, the electronic specific heat $C_e = \gamma T$ in the ferromagnetic phase [24, 25].

Therefore, it is natural to assume that the jumplike increase in the specific heat near the martensitic transformations in Heusler alloys can be explained by an increase in the density of states (DOS) near the Fermi level during the AFM (martensite)–FM (austenite) transition. To support this assumption, we calculated the DOS in an $Ni_{50}Mn_{37}In_{13}$ alloy with allowance for antiferromagnetic and ferromagnetic ordering in the martensite and austenite phases, respectively. In the antiferromagnetic ordering, the excess manganese atoms (Mn_2) located at the In sites were assumed to have a negative magnetic moment as compared to the positive magnetic moment of manganese atoms (Mn_1) that occupy the regular sites in the manganese sublattice. The electronic spectra of the cubic and tetragonal ($c/a = 1.21$) structures were calculated using the spin-polarized relativistic Korringa–Kohn–Rostoker (SPR-KKR) method and the generalized-gradient approximation (GGA) [25, 26]. The parameter of the cubic lattice with space group $Fm\bar{3}m$ ($a_0 = 0.596$ nm) was estimated by calculating lattice relaxation. The

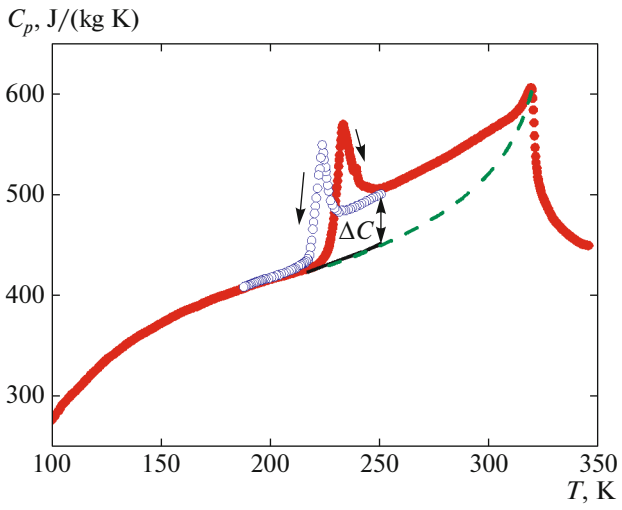

Fig. 4. (Color online) Temperature dependences of the specific heat of $Ni_{45.37}Mn_{40.91}In_{13.72}$ obtained upon heating and cooling. (dashed line) Assumed behavior of the specific heat in the absence of a magnetostructural transition.

magnetic moments calculated at Ni, Mn_1, and Mn_2 atoms in the austenite (martensite) phase are close to 0.5014, 3.668, and 3.797 (0.221, 3.637, −3.904)μ_B, respectively. The magnetic moment of Mn_2 in martensite is seen to be antiparallel to the magnetic moment of Mn_1.

Figure 5 shows the total DOSs of the austenite and martensite phases in an $Ni_{50}Mn_{37}In_{13}$ alloy that were calculated for spin-up (↑) and spin-down (↓) directions. The maxima in the spin-up and spin-down systems that are located below the Fermi level in austenite and martensite are formed by the filled 3*d* states of Ni, Mn_1, and Mn_2 atoms, and the DOS maxima that are located in the conduction band, i.e., above the Fermi level, are caused by the free 3*d* states of Mn_1 and Mn_2 atoms. Moreover, the presence of two peaks for spin-up and spin-down directions, which are above the Fermi level in martensite, is related to the antiparallel orientation of the magnetic moments of Mn_2 ($-3.904\mu_B$) and Mn_1 ($3.637\mu_B$) atoms. In contrast, one maximum for the spin-down states above the Fermi level is detected for the austenite phase with ferromagnetic ordering. The inset to Fig. 5 scales up the energy behavior of DOS for the two phases near the Fermi level. It is seen that the total DOS near the Fermi level increases during the martensite–austenite transition.

If this ideology is applied to our case, the specific heat jump ΔC detected in our experiments is in essence the difference between the electronic specific heats in the FM and AFM phases, i.e.,

$$\Delta C = \Delta C_e = (\gamma_{FM} - \gamma_{AFM})T. \quad (4)$$

The difference between the specific heats extrapolated to a temperature $T = 250$ K is $\Delta C \approx 38$ J/(kg K) (see

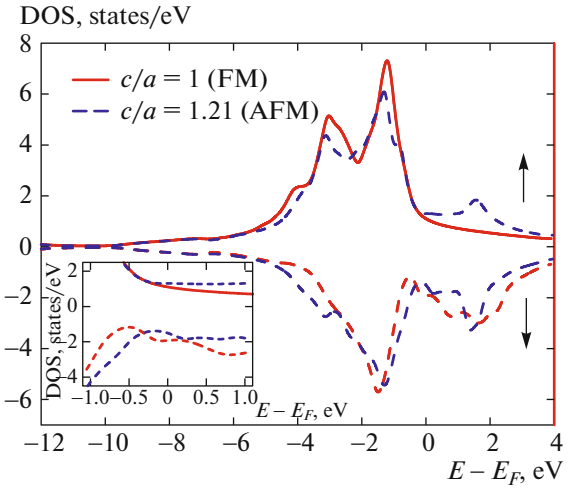

Fig. 5. (Color online) Total DOS of the $Ni_{50}Mn_{37}In_{13}$ compound for (arrow up) spin-up and (arrow down) spin-down directions. (inset) Enlarged DOS near the Fermi level. The DOSs of FM austenite ($c/a = 1$) and AFM martensite ($c/a = 1.21$) are indicated by solid and dashed lines, respectively.

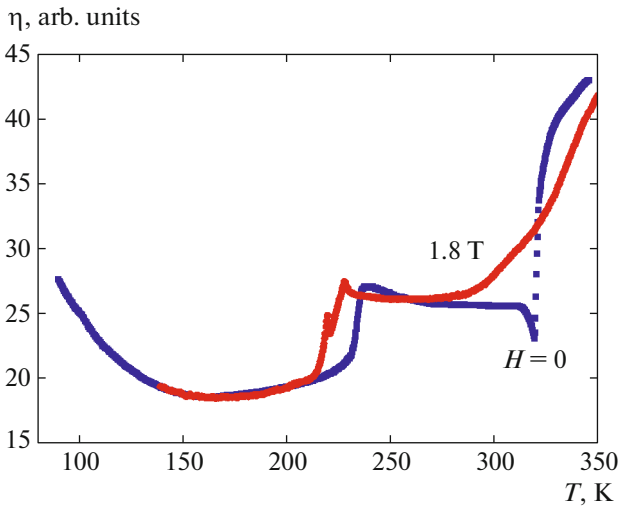

Fig. 6. (Color online) Temperature dependence of the thermal diffusion of $Ni_{45.37}Mn_{40.91}In_{13.72}$ in a zero magnetic field and a field of 1.8 T upon heating.

Fig. 4). Using coefficients $\gamma_{FM} = 8.5 \times 10^{-2}$ J/(kg K^2) and $\gamma_{AFM} = 5.4 \times 10^{-2}$ J/(kg K^2), which were obtained for an $Ni_{50}Mn_{34}In_{16.3}$ alloy from electronic specific heat [18], we can estimate the electronic specific heat jump due to a change in the DOS at the Fermi level during the AFM–FM transition. The calculations demonstrate that $\Delta C_e = 7.75$ J/(kg K) at $T = 250$ K; that is, the experimentally determined jump is higher than the jump determined from electronic specific heat by several times. To explain this discrepancy, we have to assume that the magnetic and structural subsystems also contribute to ΔC_p. Note also that a magnetic field of 1.8 T weakly affects C_p in the temperature range T_C–T_M.

Thermal diffusion is the ratio of thermal conductivity to specific heat $\eta = k/C$ and, in essence, characterizes the rate of formation of an equilibrium temperature distribution along a sample. In the case of an insulator (where phonons are the majority heat carriers), thermal diffusion determines an important physical characteristic, namely, the free path length of phonons $\eta = v_s l_{ph}/3$, where v_s is the sound velocity and l_{ph} is the mean free path of phonons.

In this case, $\eta(T)$ has no unambiguous interpretation, since k is the sum of two approximately equal quantities, i.e., $k = k_e + k_{ph}$, where k_e and k_{ph} are the electron and lattice components of the specific heat, respectively. The $\eta(T)$ curve in Fig. 6 shows, when T_C is approached from above, η decreases sharply and C_p increases but not so sharp. The small minimum at T_C is usually associated with the scattering of heat carriers by magnetic order parameter fluctuations [27]. As T decreases further, the thermal diffusion remains constant in a rather wide temperature range of 230–320 K.

η increases sharply in the martensite transformation range at $T_m = 236$. This anomaly is thought to be related to a change in the electronic specific heat, more specifically, the electrical resistivity, which changes sharply during such transformations. A magnetic field shifts T_m toward low temperatures and smoothens the anomalies at T_C, suppressing the fluctuations.

The discrepancies between the phase-transition temperatures obtained from the thermophysical (specific heat, thermal diffusion) and magnetic (magnetization) measurements can be attributed to the chemical and structural heterogeneities of the samples: C_p and η were measured on a small ($3 \times 3 \times 0.3$ mm^3) sample, and the other measurements were carried out on larger samples, though cut from the same ingot.

Figure 7 depicts the results of measuring the thermal conductivity. When measuring the thermal conductivity, we were able to determine the predominant mechanisms of scattering heat carriers in magnetic materials in various magnetic states. For functional materials, k is also a technical parameter, which is necessary to create technical devices from these materials, since it is impossible to calculate thermal balance without regard for k.

In general form, the thermal conductivity of a magnetic material can be represented as the cum of three components,

$$k_{tot} = k_e + k_{ph} + k_m,$$

where k_e, k_{ph}, and k_m are the electron, phonon, and magnetic components of the thermal conductivity. As a rule, the magnetic component is neglected because

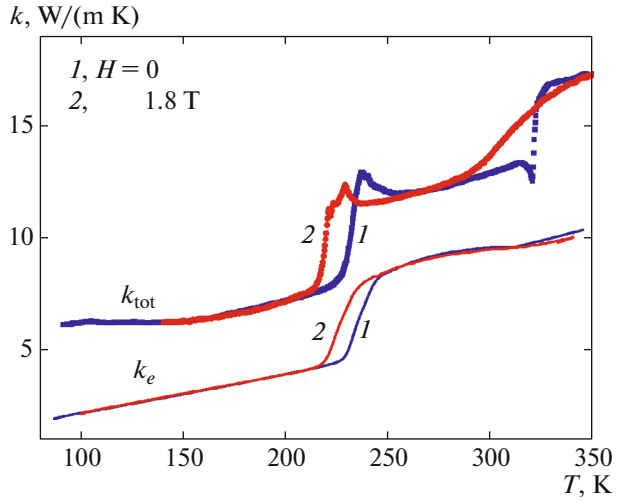

Fig. 7. (Color online) Temperature dependence of the total and electron thermal conductivities of $Ni_{45.37}Mn_{40.91}In_{13.72}$ upon heating.

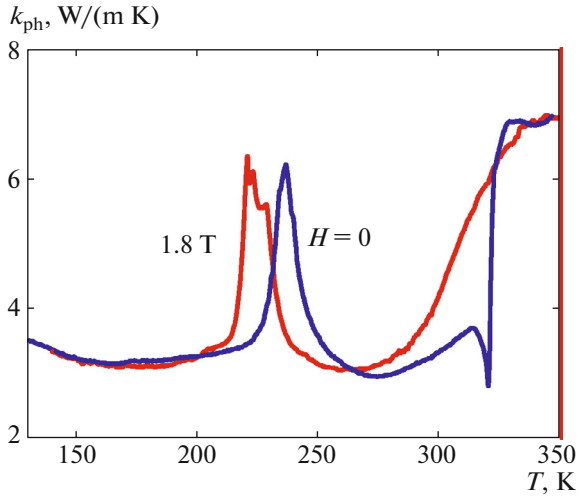

Fig. 8. (Color online) Temperature dependence of the phonon thermal conductivity of $Ni_{45.37}Mn_{40.91}In_{13.72}$ upon heating.

of its smallness [28]. Thus, the experimental $k(T)$ thermal conductivity curve shown in Fig. 6 is determined by the electron and phonon components.

In strongly diluted metallic alloys, k_e and k_{ph} can have the same order of magnitude [29]. To estimate the electron component, we can use the Wiedemann–Franz relation $k_e = L_0 T/\rho$, where $L_0 = 2.44 \times 10^{-8}$ V^2/k^2 is the Lorentz constant. In general, Lorentz number L depends on temperature; nevertheless, the assumption $L = L_0$ is valid for strongly diluted high-resistance metallic alloys this relation can be used to estimate k_e [28].

As would be expected, the behavior of $k_e(T)$ in the martensitic transformation range correlates with the behavior of $\rho(T)$: as the temperature (i.e., the fraction of austenite with a relatively high electrical conductivity) increases, k_e increases sharply and then demonstrates a smooth temperature dependence in the range $T > 230$ K. The transformation temperature corresponds to the temperature of the minimum electrical resistivity upon heating. When the temperature increases further, $k_e(T)$ remains almost constant, exhibiting a small anomaly near T_C.

The behavior of $k_{ph}(T)$, which was determined as the difference between k_{tot} and k_e calculated using the Wiedemann–Franz law, i.e., $k_{ph} = k_{tot} - k_e$, is thought to be of profound interest (Fig. 8).

The $k_{ph}(T)$ dependence is characterized by an anomalous peak near the martensite transformation temperature ($T \approx 235$ K) and a jump near T_C. This is a rare phenomenon that is unusual for metallic alloys. Anomalies in the form of small maxima caused by enhanced phonon scattering by magnetic order parameter fluctuations are usually observed during magnetic phase transitions near T_C [27]. Here, the picture is converse: the thermal conductivity increases anomalously in the form of a sharp peak near the martensitic transformation, and k_{ph} changes jumpwise near T_C.

We now discuss the peak in the $k_{ph}(T)$ dependence caused by the magnetic structural transition. In the Debye approximation, an expression for the phonon thermal conductivity has the form

$$k_{ph} = \frac{1}{3} C_p v_s l_{ph}, \qquad (5)$$

where C_p is the specific heat of phonons, v_s is the sound velocity, and l_{ph} is the free path length of phonons. In principle, each of the factors entering in the expression for k_{ph} can be responsible for the detected anomalies. However, the absorption of sound usually grows in the range of magnetic phase transitions [30]. In our case, this circumstance exerts the opposite effect; that is, it should decrease k_{ph}. Moreover, as follows from the $\eta(T)$ dependence l_{ph} cannot cause a bell-shaped increase in $k_{ph}(T)$. Thus, the detected $k_{ph}(T)$ dependence should be related to the behavior of specific heat $C_p(T)$.

Various cases of the behavior of k_{ph} in magnets were theoretically considered in [31], and it was shown that k_{ph} near phase-transition temperatures can both increase and decrease depending on the predominant mechanism of phonon scattering.

Analogous behavior of lattice thermal conductivity was only observed in a few works [32–34]. The authors of [33] studied $C_p(T)$ and $k_{ph}(T)$ of an $K_{0.3}MnO_3$ alloy, where a structural Peierls phase transition and related charge density waves take place. Both a specific heat jump ($\Delta C_p/C_p = 6\%$) and a thermal conductivity jump ($\Delta k/k = 5\%$) were detected near the Peierls phase transition, and they were thought to be associated with

an increase in the number of acoustic phonons near the transition. Larger specific heat and thermal conductivity jumps ($\Delta C_p/C_p = 26\%$, $\Delta k/k = 15\%$) were also detected near the Peierls phase transition in the $Lu_5Ir_4Si_{10}$ compound with a charge density wave. As in the case of $K_{0.3}MnO_3$, they were interpreted in terms of a model according to which the Peierls transition [34] is accompanied by the appearance of additional soft phonon modes.

The martensitic transition in Heusler alloys has many common features with the Peierls phase transition. In both cases, the structural transitions are accompanied by the softening of a phonon spectrum and the appearance of a large number of addition thermal excitations, which increase C_p. As a result, the quantity of heat carried by such phonons also grows, since their frequency corresponds to the acoustic branch of phonons, which are responsible for thermal conductivity.

These concepts were used the authors of [32] to explain the very sharp changes in the thermal conductivity of $Ni_{2-x}Mn_{1-x}Ga$ Heusler alloys near the martensitic transformations in them. Note that the relative change in the thermal conductivity of these alloys at $x = 0.18$, where structural and magnetic phase transitions coincide ($T_C = T_m = 320$ K), reaches giant values (about 100%), although the specific heat jump is not so high.

This ideology can also be used to interpret our experimental data, according to which the anomalous growth of k_{ph} is $\Delta k_{ph}/k_{ph} \approx 70\%$ and takes place at $T \approx 233$ K, which approximately coincides with $A_f = 231$ K. A thermal conductivity jump of $\Delta C_p/C_p = 34\%$ also occurs at this temperature. The fact that the thermal conductivity peak is determined by not only changes in the specific heat is seen from both a comparison of the changes in the specific heat and the thermal conductivity and the fact that C_p before and after the transition cannot be approximated by one continuous line and the values of k_{ph} before and after the transition are approximately the same. This finding indicates that there exists a certain additional mechanism increasing the thermal conductivity. The fact that an increase in the free path length of phonons during a martensitic transformation can contribute to this process was noted in [35].

The causes of the sharp increase in the thermal conductivity and the thermal diffusion near T_C can only be discussed. A similar increase in the thermal conductivity of an $Ni_{50}Mn_{34}In_{16}$ alloy ($\Delta k/k \approx 70\%$) was detected near T_C in [36], and this anomalous increase was attributed to changes in the electron component of the thermal conductivity (but $\rho(T)$ curve was not presented).

In our case, this assumption is erroneous because of the absence of sharp anomalies in the behavior of $\rho(T)$ near T_C. This behavior is assumed to be related to the structural changes that occur near T_C: the appearance of a less symmetric tetragonal phase (martensite) in an austenite matrix can mean the appearance of an additional phonon relaxation channel and can result in the determined $k_{ph}(T)$ and $\eta(T)$ dependences. The coexistence of the austenite and martensite phases near T_C in an $Ni_{50}Mn_{35}In_{15}$ alloy also follows from the results in [37].

CONCLUSIONS

The electrical, thermal, and magnetic properties of an $Ni_{45.37}Mn_{40.91}In_{13.72}$ alloy were studied. The detected anomalies in the properties are related to martensitic transformations and their dependences on the magnetic field and temperature. The behavior of magnetization corresponds to the model in which the low-temperature martensite phase is mainly antiferromagnetic with insignificant inclusions of a ferromagnetic phase. The experimental data on differential scanning calorimetry, specific heat, and magnetization suggest that the phase transition detected at T_C if a first-order magnetostructural phase transition. The jumplike increase in the specific heat and the sharp decrease in the electrical resistivity near the martensitic transformations are partly related to an increase in the DOS near the Fermi level during the AFM (martensite)–FM (austenite) transition. The anomalously high thermal conductivity of phonons near the martensitic transition can be explained by the appearance of soft phonon modes, which make an additional contribution to C_p and k_{ph}.

ACKNOWLEDGMENTS

We thank Z.Z. Alisultanov for helpful discussions.

Some investigations were carried out on the equipment of the Analytical Center of Joint Use of the Dagestan Research Center, Russian Academy of Sciences.

This work was performed in terms of the program Strongly Correlated Electrons in Solids and Structures of the Department of Physical Sciences of the Russian Academy of Sciences and was supported by the Russian Foundation for Basic Research (project nos. 14-02-01177, 12-02-96506).

REFERENCES

1. V. D. Buchelnikov, A. N. Vasil'ev, S. V. Taskaev, V. V. Koledov, S. V. Taskaev, V. V. Khovaylo, and V. G. Shavrov, Phys. Usp. **49**, 871 (2006).
2. V. D. Buchelnikov, S. V. Taskaev, M. A. Zagrebin, and P. Entel, JETP Lett. **85**, 560 (2007).
3. V. V. Khovaylo, T. Kanomata, T. Tanaka, M. Nakashima, Y. Amako, R. Kainuma, R. Y. Umetsu, H. Morito, and H. Miki, Phys. Rev. B **80**, 144409 (2009).

4. L. H. Bennett, V. Provenzano, R. D. Shull, I. Levin, E. della Torre, and Y. Jin, J. Alloys Comp. 525, 34 (2012).
5. H. M. Seyoum, M. Ghahremani, H. Eibidweihy, L. H. Bennett, E. della Torre, F. Johnson, and M. Zuo, IEEE Magn. Lett. **4**, 6000204 (2013).
6. A. N. Vasil'ev, V. D. Buchel'nikov, T. Takagi, V. V. Khovailo, and E. I. Estrin, Phys. Usp. **46**, 559 (2003).
7. P. F. Sullivan and G. Seidel, Phys. Rev. **173**, 679 (1968).
8. R. Kainuma, Y. Imano, W. Ito, Y. Sutou, H. Morito, S. Okamoto, O. Kitakami, K. Oikawa, A. Fujita, T. Kanomata, and K. Ishida, Nature **439**, 957 (2006).
9. I. Dubenko, A. K. Pathak, N. Ali, Ya. Kovarskii, V. N. Prudnikov, N. S. Perov, and A. B. Granovsky, J. Phys.: Conf. Ser. **200**, 052005 (2010).
10. Y. Sutou, Y. Imano, N. Koeda, Y. Omori, R. Kainuma, K. Ishida, and K. Oikawa, Appl. Phys. Lett. **85**, 4858 (2004).
11. I. Dubenko, M. Khan, A. K. Pathak, B. R. Gautam, S. Stadler, and N. Ali, J. Magn. Magn. Mater. **321**, 754 (2009).
12. A. K. Pathak, B. R. Gautam, I. Dubenko, M. Khan, S. Stadler, and N. Ali, J. Appl. Phys. 103, 07F315 (2008).
13. A. Planes, L. Manosa, and M. Acet, J. Phys.: Cond. Mat. **21**, 233201 (2009).
14. Yu. V. Kaletina and E. G. Gerasimov, Phys. Solid State **56**, 1634 (2014).
15. K. Oikawa, W. Ito, Y. Imano, Y. Sutou, R. Kainuma, K. Ishida, S. Okamoto, O. Kitakami, and T. Kanomata, Appl. Phys. Lett. **88**, 122507 (2006).
16. V. N. Prudnikov, A. P. Kazakov, I. S. Titov, N. S. Perov, A. B. Granovskii, I. S. Dubenko, A. K. Patak, N. Ali, A. P. Zhukov, and Kh. Gonzales, JETP Lett. **92**, 666 (2010).
17. I. Dubenko, A. K. Pathak, S. Stadler, and N. Ali, Phys. Rev. B **80**, 092408 (2009).
18. B. Zhang, X. X. Zhang, S. Y. Yu, J. L. Chen, Z. X. Cao, and G. H. Wu, Appl. Phys. Lett. **91**, 012510 (2007).
19. A. N. Vasiliev, O. Heczko, O. S. Volkova, T. N. Vasilchikova, T. N. Voloshok, K. V. Klimov, W. Ito, R. Kainuma, K. Ishida, K. Oikawa, and S. Fahler, J. Phys. D: Appl. Phys. **43**, 055004 (2010).
20. I. Dubenko, A. K. Pathak, A. Kazakov, T. Samanta, V. Prudnikov, S. Stadler, A. R. Granovsky, A. Zhukov, and N. Ali, J. Magn. Magn. Mater. **324**, 3530 (2012).
21. S. M. Podgornykh, E. G. Gerasimov, N. V. Mushnikov, and T. Kanomata, J. Phys.: Conf. Ser. **266**, 12004 (2011).
22. V. K. Sharma, M. K. Chattopadhyay, R. Kumar, T. Ganguli, P. Tiwari, and S. B. Roy, J. Phys.: Condens. Matter **19**, 496207 (2007).
23. X. Moya, L. Manosa, and A. Planes, Phys. Rev. B **75**, 184412 (2007).
24. P. Tu and A. J. Heeger, J. Appl. Phys. **40**, 1368 (1969).
25. D. W. Cooke and F. Hellman, Phys. Rev. Lett. **109**, 255901 (2012).
26. H. Ebert, D. Ködderitzsch, and J. Minár, Rep. Prog. Phys. **74**, 096501 (2011); SPR-KKR Package, Version 6.3. http://ebert.cup.uni-muenchen.de.
27. A. M. Aliev, A. B. Batdalov, and A. G. Gamzatov, J. Low Temp. Phys. **36**, 171 (2010).
28. J. L. Cohn, J. J. Neumeier, C. P. Popoviciu, K. J. McClellan, and Th. Leventouri, Phys. Rev. B **56**, R8495 (1997).
29. R. Berman, *Heat Conductivity of Solids* (Mir, Moscow, 1979).
30. V. D. Buchelnikov and V. G. Shavrov, Phys. Solid State **37**, 760 (1995).
31. V. D. Buchelnikov, Yu. A. Kuzavko, and V. G. Shavrov, Sov. J. Low Temp. Phys. **13**, 611 (1987).
32. Y. K. Kuo, K. M. Sivakumar, H. C. Chen, J. H. Su, and C. S. Lue, Phys. Rev. B **72**, 054116 (2005).
33. R. S. Kwok and S. E. Brown, Phys. Rev. Lett. **63**, 895 (1989).
34. C. S. Lue, Y. Kuo, F. H. Hsu, H. H. Li, H. D. Yang, P. S. Fodor, and L. E. Wenger, Phys. Rev. B **66**, 033101 (2002).
35. A. M. Aliev, A. B. Batdalov, L. N. Khanov, V. D. Buchel'nikov, S. V. Taskaev, et al., in *Proceedings of the 8th International Seminar on Magnetic Phase Transitions* (Makhachkala, 2007), p. 56.
36. L. S. Sharath Chandra, M. K. Chattopadhyay, V. K. Sharma, and S. B. Roy, Phys. Rev. B **81**, 195105 (2010).
37. I. D. Rodionov, Yu. S. Koshkid'ko, J. Cwik, A. Quetz, S. Pandey, A. Aryal, I. S. Dubenko, S. Stadler, N. Ali, I. S. Titov, M. Blinov, M. V. Prudnikova, V. N. Prudnikov, E. Lahderanta, and A. B. Granovskii, JETP Lett. **101**, 385 (2015).

Translated by K. Shakhlevich